Materials and Design 88 (2015) 222–226

Contents lists available at ScienceDirect

Materials and Design

journal homepage: www.elsevier.com/locate/jmad

Evaluation of glass formation and critical casting diameter in Al-based metallic glasses

J.P. Liao [a], B.J. Yang [a], Y. Zhang [a], W.Y. Lu [a], X.J. Gu [b], J.Q. Wang [a,*]

[a] Shenyang National Laboratory for Materials Science, Institute of Metal Research, CAS, Shenyang 110016, PR China
[b] Department of Mechanical Engineering, One Dent Drive, Bucknell University, Lewisburg, PA 17837, USA

ARTICLE INFO

Article history:
Received 22 July 2015
Received in revised form 26 August 2015
Accepted 27 August 2015
Available online 5 September 2015

Keywords:
Al-based bulk metallic glasses
Critical cooling rate
Copper-mold casting

ABSTRACT

Critical cooling rate R_c for a series of Al-based glass formers, as well as cooling rate T' for copper-mold casting Al-based bulk metallic glass (BMG) samples, have been calculated. It is found that the glass forming ability (GFA) is reflected by the change of R_c value, and $Al_{86}Ni_6Y_{4.5}Co_2La_{1.5}$ alloy, the best glass former in Al-based systems, holds the lowest R_c of about 3.01×10^3 K/s. The T' for the rod sample is determined by casting diameter D. When synthesizing Al-based BMGs, with the D increases from 1 mm to 3 mm, the value of T' decreases from 7.48×10^3 K/s to 0.83×10^3 K/s. Based on these calculations, the critical casting diameter D_c for a certain Al-rich multi-composition could be predicted. Further, for the composition $Al_{86}Ni_6Y_{4.5}Co_2La_{1.5}$, bulk glassy sample with D_c up to 1.5 mm has been obtained, confirming the theoretical prediction.

1. Introduction

Al-based metallic glasses, with their ultra-high specific strength [1] and good corrosion resistance [2], have been considered as important potential engineering materials [3,4]. Since Al-based metallic glass was discovered in 1988 [5], numerous efforts have been devoted to developing Al-based lightweight bulk glassy alloys [1,6–10]. Owing to its low glass forming ability (GFA), the largest size of Al-based bulk metallic glass (BMG) reported so far is only 1 mm [1]. The size limitation of Al-based metallic glasses has hindered its further development in many relevant areas, such as the optional design of microstructure [9,11], the investigation of corrosion-resisting properties with large scale metallic coatings [4] and the mechanical properties investigation of BMGs with selective laser melting (SLM) technique [12–14] *etc.* In order to design larger Al-based BMG to fulfill its potential application, many methods, *e.g.*, theoretical models [6,7,15,16] and empirical criterions [1,8], have been proposed. Unfortunately, solidification process, another key factor closely related to sample size, has rarely been analyzed in Al-based BMGs in previous researches. It will be crucial for pushing engineering application of Al-based metallic glasses. Therefore, it is highly desirable to further understand the solidification process and uncover the glass formation mechanism of Al-based BMGs.

GFA can be viewed as the resistance to the precipitation of crystalline phases during solidification process. For many typical bulk glass-former systems, their solidification processes have been investigated systematically. For example, the influence of casting parameters on the critical casting size was investigated for systems based on Ca and Mg by Laws et al. [17], the microstructure and kinetic transitions for Fe-based BMG during solidification process were analyzed by Perepezko and Hildal [18], and the time-temperature-transformation (TTT) diagram, constructed experimentally in Zr-based glass forming alloy, was used to investigate crystallization and phase separation behavior by Kim et al. [19]. However, due to size limitation of Al-based metallic glasses, experimental investigation of the solidification process is extremely difficult. It seems to be applicable to analyze their solidification process and formation characteristics by means of theoretical calculation methods. In fact, some calculation methods have been used for many BMG-forming systems successfully, such as the critical cooling rate evaluation based on the thermodynamics [20–22], the cooling rate estimation according to the Fourier's law [23–25], and the mixing enthalpy and mismatch entropy calculation for evaluating GFA [26].

In this paper, our purpose is to understand the characteristics of solidification process and its relationship with glass forming in a series of Al-based metallic glass systems on the basis of theoretical calculations. Correspondingly, the critical casting diameters D_c for Al-based BMGs are predicted theoretically and further verified experimentally.

2. Critical cooling rate and critical casting diameter estimation for Al-based metallic glasses

2.1. Critical cooling rate calculation

GFA can be directly reflected and assessed by critical cooling rate R_c. The smaller the R_c is, the higher the GFA will be. To define GFA of a certain alloy, R_c should be obtained first. Unfortunately, experimental investigation of R_c for Al-based metallic glasses is extremely difficult due to the size limitation. In this case, theoretical calculation method seems to be an applicable way.

* Corresponding author.
E-mail address: jqwang@imr.ac.cn (J.Q. Wang).

http://dx.doi.org/10.1016/j.matdes.2015.08.138
0264-1275/

In 1968, a formula used to calculate R_c of traditional oxide glasses was given by Sarjeant and Roy [20]:

$$R_c = Z\frac{k_B T_l^2}{a^3 \eta_{T_l}} \tag{1}$$

where Z is a constant of 2×10^{-6}, k_B is the Boltzmann constant, a is the interatomic distance, T_l is the liquidus temperature and η_{T_l} is the viscosity at T_l.

Owing to the limitation of Eq. (1), an equation that can reasonably estimate R_c for glass formation in multi-component alloy systems was required. In this case, derived from Eq. (1), Takeuchi and Inoue proposed a modified equation by adding a correction factor of $\exp(\Delta G/RT)$ [21]:

$$R_c = Z\frac{k_B T_l^2}{a^3 \eta_{T_l}} exp\left(\frac{\Delta G}{RT}\right) \tag{2}$$

where R is the gas constant and ΔG is the free energy of mixing which can be obtained by the regular solution model [26].

In order to evaluate R_c, several parameters have to be determined. The equations for calculating the values of these parameters are shown as follows:

$$a = \sum_{i=1}^{N} C_i a_i \tag{3}$$

$$\eta_{T_l} = 10^{-3.3}\, exp\left(\frac{3.34 T_l}{T - T_g}\right) \tag{4}$$

where C_i is the atomic mass fraction of ith element, η_{T_l} is often approximated by Eq. (4), an empirical equation which has been verified in many metallic glass systems [27], T_g is the glass transition temperature, T_l and T_g can be obtained from experimental data.

Based on Eq. (2), the estimated R_c for various Al-based metallic glass systems can be achieved. Table 1 shows the calculated R_C for different alloy compositions and summarizes the parameters which are needed for the calculation. In order to verify the validity of the calculation method, the maximum size of fully amorphous samples (t_c) obtained with different preparation techniques are also listed.

As shown in Table 1, the values of R_c for the typical Al-based metallic glasses are in the range of 10^3 K/s to 10^4 K/s, which is comparable to that ever estimated from experimental experience. As expected, the composition of $Al_{86}Ni_6Y_{4.5}Co_2La_{1.5}$, with the best GFA, has the minimum R_c of about 3.01×10^3 K/s, while the composition of $Al_{87}Ni_9Ce_4$ has the maximum R_c of nearly 1.02×10^4 K/s. It indicates that the R_c agrees well with the GFA. More specifically, the calculation results show a tendency that R_c decreases with the number of component increases. Overall, for a certain Al-rich multi-component system, there exists a similar variation tendency between R_c and t_c. In most cases, the t_c corresponds to the lowest R_c. It implies that the calculation method used above is applicable for Al-based metallic glasses.

The effect of the free energy of mixing ΔG on the critical cooling rate R_c has also been analyzed in this work. For clarity, the values of ΔG and R_c for various Al-based alloys obtained by calculating are plotted in Fig. 1. It can be clearly seen that the Al-based alloy with a large negative value of ΔG has an apparent decreasing tendency in R_c,which means the alloy with a larger value of ΔG is much more beneficial to form glassy phase. However, not all compositions agree well with such variation trends between ΔG and R_c, such as the alloy $Al_{87.5}Ni_4Sm_{8.5}$ and $Al_{85}Ni_5Fe_2Gd_8$. In addition, seen from Fig. 1, there exists an overlapped area between ternary and quaternary alloy systems, and between quaternary and quinary alloy systems as well. Apparently, for Al-based alloy systems, some ternary alloys, as the example of $Al_{85.5}Ni_{9.5}Ce_5$, may have better GFA than some quaternary alloys, and the similar situation occurs between quaternary and quinary alloys, like $Al_{86}Ni_8Y_{4.5}La_{1.5}$.

2.2. Cooling rate calculation for copper-mold casting process

For a cylindrical-shaped metallic glass produced by copper-mold casting, during the solidification process, heat transfer takes place by conduction from the molten metal to the contacted copper mold. To date, many theories on the heat transfer of copper-mold casting process have been proposed, and numerous efforts have been made to understand the solidification process [17,18,28,29]. However, instead of intensive study of the casting process, this work focuses on simplifying

Table 1
Calculated results based upon the reference-reported data in a series of Al-based metallic glasses.

Alloy	a (Å)	T_g (K)	T_l (K)	η_{T_l} (Pa s)	ΔG ($\times 10^4$ J/mol)	R_c (K/s)	t_c (μm)	Refs.
$Al_{87.5}Ni_4Sm_{8.5}$	2.60	508	1268	0.13	−1.95	7.20×10^3	–	[32]
$Al_{85.6}Ni_{9.2}Sm_{5.2}$	2.68	505	1198	0.16	−1.93	5.24×10^3	–	[15]
$Al_{87}Ni_7Gd_6$	2.66	488	1167	0.16	−1.86	7.01×10^3	300^R	[33]
$Al_{85.7}Ni_{9.1}Gd_{5.2}$	2.68	510	1200	0.17	−1.94	4.89×10^3	–	[34]
$Al_{87}Ni_9Ce_4$	2.86	468	1146	0.14	−1.73	1.02×10^4	290^W	[35]
$Al_{87}Ni_8Ce_5$	2.87	496	1142	0.18	−1.78	6.23×10^3	400^W	[35]
$Al_{85}Ni_{10}Ce_5$	2.86	523	1165	0.22	−1.84	4.45×10^3	425^W	[35]
$Al_{85.5}Ni_{9.5}Ce_5$	2.86	519	1158	0.21	−1.90	3.49×10^3	510^W	[35]
$Al_{85.8}Ni_{9.1}Ce_{5.1}$	2.87	484	1185	0.14	−1.91	5.16×10^3	–	[34]
$Al_{88}Co_4Y_8$	2.91	507	1189	0.17	−1.82	6.03×10^3	200^R	[40]
$Al_{88}Co_5Y_7$	2.89	522	1193	0.19	−1.76	6.99×10^3	230^R	[36]
$Al_{85.8}Co_{9.1}Y_{5.1}$	2.87	516	1230	0.16	−1.83	7.05×10^3	–	[34]
$Al_{85.8}Ni_{9.1}Y_{5.1}$	2.86	477	1200	0.13	−1.92	5.62×10^3	180^R	[34,40]
$Al_{86}Ni_8Y_6$	2.87	494	1201	0.15	−1.96	4.16×10^3	260^R	[34]
$Al_{88}Ni_4Y_8$	2.90	465	1189	0.12	−1.87	6.86×10^3	200^R	[40]
$Al_{85}Ni_{10}La_5$	2.87	510	1177	0.18	−1.91	4.06×10^3	580^W	[37]
$Al_{86}Ni_9La_5$	2.87	498	1115	0.21	−1.86	3.97×10^3	685^W	[8,37]
$Al_{85}Ni_6Fe_3Gd_6$	2.58	570	1173	0.33	−1.85	3.82×10^3	250^R	[38]
$Al_{85}Ni_5Fe_2Gd_8$	2.56	570	1283	0.20	−2.03	3.65×10^3	200^R	[38]
$Al_{86}Ni_6Y_6Co_2$	2.87	512	1207	0.17	−1.99	3.38×10^3	850^W	[34]
$Al_{86}Ni_8Y_{4.5}La_{1.5}$	2.88	507	1206	0.16	−2.00	3.30×10^3	785^W	[34]
$Al_{86}Ni_7Y_5Co_1La_1$	2.88	500	1205	0.15	−2.01	3.32×10^3	1000^C	[34]
$Al_{86}Ni_7Y_{4.5}Co_1La_{1.5}$	2.88	504	1196	0.16	−2.01	3.04×10^3	1000^C	[34]
$Al_{86}Ni_6Y_{4.5}Co_2La_{1.5}$	2.88	505	1197	0.16	−2.02	3.01×10^3	1000^C	[34]

t_c is the experimental critical size, and superscript R is for melt-spinning, W is for wedge-shaped casting, C is for cylindrical-shaped casting.

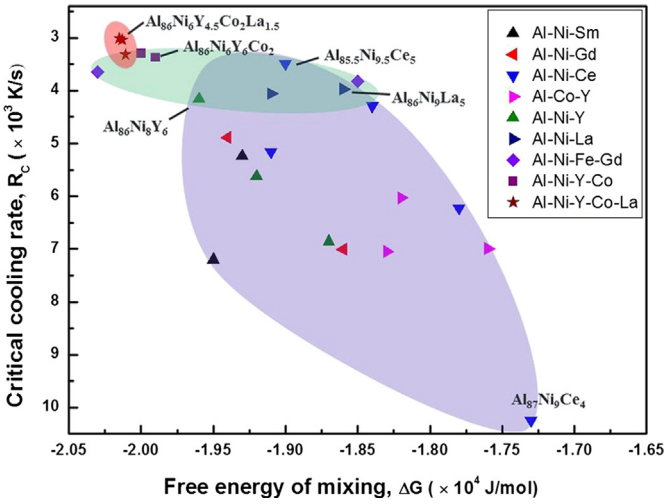

Fig. 1. Illustration of the relationship between critical cooling rate R_c and free energy of mixing ΔG for Al-based metallic glasses, the triangles, the quadrangles and the pentagrams correspond to the ternary, the quaternary and the quinary alloy systems, respectively.

the heat transfer process of copper-mold casting so as to generate an expression that can reasonably estimate the cooling rate.

Here are the simplified treatments for the heat transfer in the copper-mold casting process. There is no gap between the casting rod and the copper mold, so that only heat conduction is considered. For the cylindrical-shaped copper mold, heat transfer process can be regarded as one dimension conduction which is consistent with the Fourier's law. The latent heat of crystallization is neglected since no crystal is formed during cooling. The physical properties of the Al-based alloys and the copper mold used in the calculation are constant, and are independent of temperature.

Based on these simplifications, the solidification process can be considered at a relatively ideal state. According to a series of theoretical derivations deduced by Wang et al. [24], the cooling rate expression for the center area of the cylindrical-shaped molten metal was eventually proposed:

$$[T_1']_{x=-r} = \frac{(b_2T_{20} - b_2T_{10})e^{-\frac{K^2}{\alpha_1}} \cdot K^3}{(b_1 + b_2)\sqrt{\alpha_1} \cdot r^2} \tag{5}$$

where $[T_1']_{x=-r}$ is the cooling rate at the sample center, r is the radius of the casting rod, b_1 and b_2 are the coefficients of thermal storage of the alloy and the copper mold, K is the Chvorinov's constant, and the subscripts 0, 1, 2 denote the initial condition, the rod sample and the copper mold, respectively. Eq. (5) describes the cooling rate variation with radius. Herein, the temperatures T_{10} and T_{20} can be obtained once the experimental condition is determined, and all the other parameters are considered as constants for a certain alloy composition.

For Al-based BMGs, parameters needed for the calculation are listed in Table 2. Based on Eq. (5), the calculation results are shown in Table 3, the results indicate that with the casting diameter D, which equals to $2r$, increases from 1 mm to 3 mm, the cooling rate for the center area decreases from 7.48×10^3 K/s to 0.83×10^3 K/s, which means the larger the sample size is, the lower the cooling rate will be. Meanwhile, it can be seen from Table 3 that for the 1.5 mm diameter sample, the obtained cooling rate for copper mold casting is about 3.32×10^3 K/s; while for the 3 mm diameter sample, the cooling rate turns out to be 0.83×10^3 K/s which falls to below 10^3 K/s. Clearly, with the increase of the casting diameter, the cooling rate drops rapidly.

Table 3
The cooling rate obtained by calculation corresponding to the casting diameter.

Casting diameter, D (mm)	1.0	1.5	2.0	3.0
Cooling rate, T' (K/s)	7.48×10^3	3.32×10^3	1.87×10^3	0.83×10^3

2.3. Critical casting diameter prediction

A useful kinetic analysis for solidification process is the evaluation of TTT curve, where the position of the nose of the transformation curve, corresponding to the value of R_c, is used to avoid nucleation and growth. According to Eq. (2), the values of R_c for different glass-forming alloys can be obtained. Thus, the position of the nose area of a schematic TTT curve for a certain alloy can be speculated based on the calculated R_c [18,30]. To relate the solidification characteristics to the calculated R_c, the continuous-cooling-transformation (CCT) curve should be obtained as well. Eq. (5) expresses the correlation between the cooling rate and the casting size for copper-mold casting process. Based on the calculated results, the CCT curves could be constructed.

In the analysis of glass formation, TTT curves have to be used in combination with CCT curves. The onset time for crystallization is the moment when the CCT curve just passes through the nose of the TTT curve, and if the CCT curve bypasses the nose, metallic glass structure will form [18,31]. Obviously, the kinetic analysis of solidification process can be investigated by using the information from the calculated TTT and CCT curves. The resulting CCT/TTT diagrams for Al-based glass forming alloys, based on Section 2.1 and Section 2.2, are shown in Fig. 2. The TTT curves for three typical Al-based glass forming alloys, $Al_{86}Ni_8Y_6$, $Al_{86}Ni_6Y_6Co_2$ and $Al_{86}Ni_6Y_{4.5}Co_2La_{1.5}$, were schematically drawn according to the theoretically calculated results of R_c. The CCT curves were constructed for the calculated T', corresponding to the casting diameter of 1 mm, 1.5 mm, 2 mm and 3 mm, respectively. Clearly, with the increase of alloying element, the corresponding TTT curve moves to the right side. It reflects the alloy presents much better GFA with the increased number of components. This is exactly required for a lower T' or a relatively larger D when synthesizing BMGs. Note that the critical casting diameter D_c could be predicted theoretically with the combination of TTT and CCT curves.

As we know, numerous efforts have been made to design better Al-based glass formers [1,8,15,32–38], and the Al–Ni–Y–Co–La quinary alloy system presents the best GFA [1,34]. Deduced from Table 1, herein, we selected $Al_{86}Ni_6Y_{4.5}Co_2La_{1.5}$ alloy for the following study since it has the minimum R_c (*i.e.* the best GFA) compared with other quinary alloy compositions.

Clearly, from Fig. 2, the nose of the TTT curve for $Al_{86}Ni_6Y_{4.5}Co_2La_{1.5}$ falls in the interval between 1.87×10^3 K/s and 3.32×10^3 K/s, corresponds to D_c in the range of 1.5 mm to 2 mm. Note that the calculation

Table 2
Parameters used for calculating the cooling rate of the copper-mold casting [25].

Materials	Thermal conductivity, k (W/(m K))	Specific heat capacity, C_p (J/(kg K))	Density, P (kg/m^3)	Thermal diffusivity, α ((W m^2)/J)	Temperature, T_0 (K)
Al-based alloy	94	1080	2385	3.6×10^{-5}	1197
Cu mold	398	384	8900	1.2×10^{-4}	298

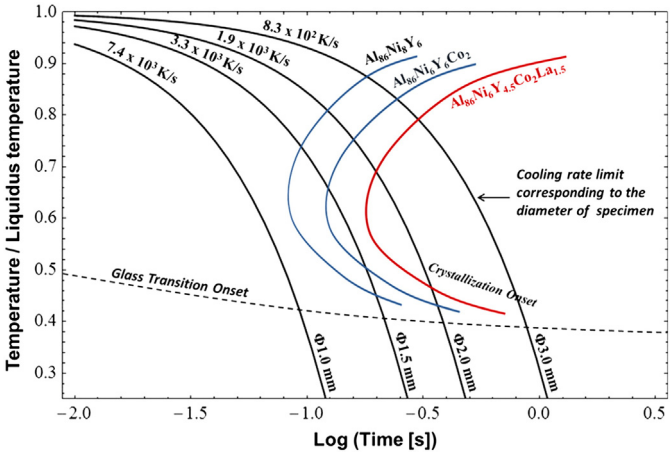

Fig. 2. Schematic CCT/TTT diagram based on the calculated results [39]. The CCT curves correspond to the casting diameter of Al-based BMGs and the TTT curves are plotted for three typical Al-based metallic glasses: $Al_{86}Ni_8Y_6$, $Al_{86}Ni_6Y_6Co_2$ and $Al_{86}Ni_6Y_{4.5}Co_2La_{1.5}$.

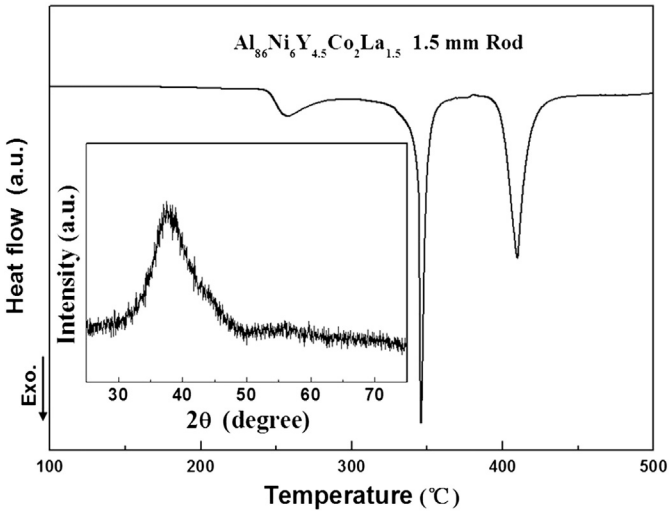

Fig. 4. DSC curve of the amorphous part of the $Al_{86}Ni_6Y_{4.5}Co_2La_{1.5}$ alloy rod with 1.5 mm in diameter, the inset XRD pattern indicates its amorphous nature.

models constructed above were at ideal states and some simplifications have been made. Although some influencing factors should be taken into consideration in practice, it still could be expected to cast a cylindrical-shaped sample with 1.5 mm in diameter.

3. Experimental verification

To confirm the above analysis, the copper-mold casting experiment of $Al_{86}Ni_6Y_{4.5}Co_2La_{1.5}$ alloy has been performed. Fig. 3a shows the cross-sectional SEM micrograph for the alloy $Al_{86}Ni_6Y_{4.5}Co_2La_{1.5}$ with 1.5 mm diameter, the inset image is the outer appearance of the glassy part of the rod. From the magnified image in Fig. 3b, clearly, no crystalline grain can be found, indicating a fully amorphous structure.

Fig. 4 presents the DSC and XRD profiles of the cross section of the glassy part. Obviously, no observable crystalline peak is found in the X-ray pattern. The DSC and XRD results of the composition $Al_{86}Ni_6Y_{4.5}Co_2La_{1.5}$ confirm its amorphous nature. Moreover, the high-resolution TEM image and the inset selected-area electron diffraction (SAED) pattern for alloy $Al_{86}Ni_6Y_{4.5}Co_2La_{1.5}$ are presented in Fig. 5. The sample was taken from the center of the 1.5 mm as-cast rod. The broad halo in the SAED pattern indicates the presence of a single glassy phase and no crystal is visible in the high-resolution TEM image which agrees well with the XRD result that the sample is completely non-crystal. The results verified that the critical casting diameter prediction is practicable and the calculation methods are reasonable.

4. Conclusions

The critical cooling rates R_c for typical Al-based glass forming alloys were estimated. The values of R_c vary from 3.01×10^3 K/s to 1.02×10^4 K/s, and Al-based alloy with a large negative value of ΔG has an apparent decreasing tendency in R_c. The cooling rates T' of Al-based BMGs during copper-mold casting were calculated. The values of T' decrease from 7.48×10^3 to 0.83×10^3 K/s as the casting diameter increase from 1 mm to 3 mm. The theoretical calculations present that $Al_{86}Ni_6Y_{4.5}Co_2La_{1.5}$, with the minimum R_c, can be casted into fully-amorphous sample with 1.5 mm in diameter and the experimental results confirmed this prediction.

Acknowledgments

This work was supported by the National Nature Science Foundation of China (Nos. 51131006, 51471166). The authors are also grateful to Dr. S. Li and Dr. X.Y San for the assistance in TEM observations.

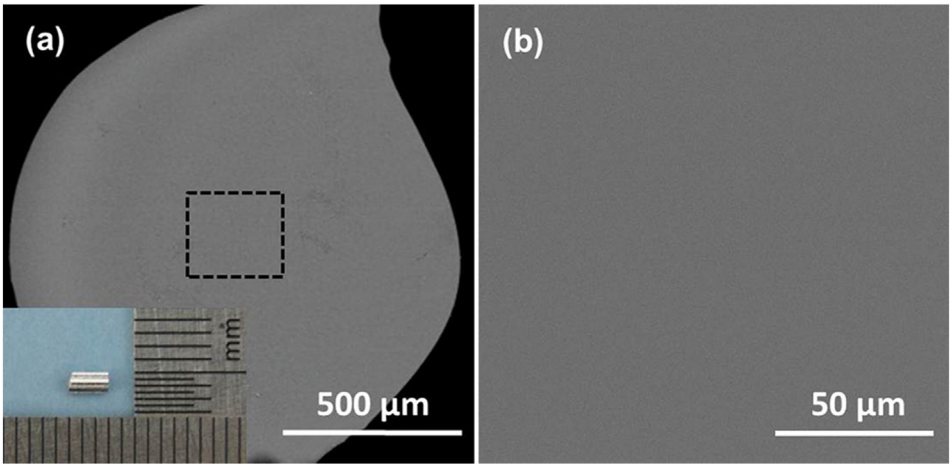

Fig. 3. SEM micrograph of $Al_{86}Ni_6Y_{4.5}Co_2La_{1.5}$ alloy: (a) Micrograph corresponding to the cross section of a 1.5 mm diameter rod and the inset image is the appearance of the amorphous part; (b) magnified image of the detail marked in Panel a.

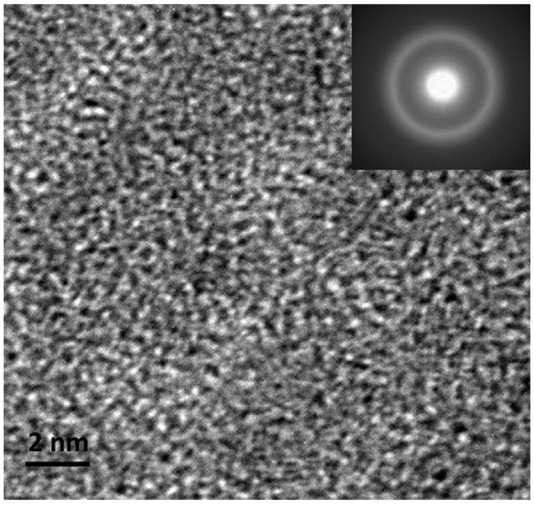

Fig. 5. High-resolution TEM image of the 1.5 mm diameter $Al_{86}Ni_6Y_{4.5}Co_2La_{1.5}$ alloy rod. The inset image shows the corresponding SAED pattern.

References

[1] B.J. Yang, J.H. Yao, J. Zhang, H.W. Yang, J.Q. Wang, E. Ma, Al-rich bulk metallic glasses with plasticity and ultrahigh specific strength, Scr. Mater. 61 (2009) 423–426.

[2] S.D. Zhang, Z.W. Liu, Z.M. Wang, J.Q. Wang, In situ EC-AFM study of the effect of nanocrystals on the passivation and pit initiation in an Al-based metallic glass, Corros. Sci. 83 (2014) 111–123.

[3] A. Inoue, H. Kimura, Fabrications and mechanical properties of bulk amorphous, nanocrystalline, nanoquasicrystalline alloys in aluminum-based system, J. Light. Met. 1 (2001) 31–41.

[4] F. Presuel-Moreno, M.A. Jakab, N. Tailleart, M. Goldman, J.R. Scully, Corrosion-resistant metallic coatings, Mater. Today. 11 (2008) 14–23.

[5] Y. He, S.J. Poon, G.J. Shiflet, Formation and stability of aluminum-based metallic glasses in Al–Fe–Gd alloys, Scr. Met. Mater. 22 (1988) 1813–1816.

[6] H.W. Sheng, W.K. Luo, F.M. Alamgir, J.M. Bai, E. Ma, Atomic packing and short-to-medium-range order in metallic glasses, Nature 439 (2006) 419–425.

[7] H.W. Sheng, Y.Q. Cheng, P.L. Lee, S.D. Shastri, E. Ma, Atomic packing in multicomponent aluminum-based metallic glasses, Acta Mater. 56 (2008) 6264–6272.

[8] C.S. Ma, J. Zhang, X.C. Chang, W.L. Hou, J.Q. Wang, Electronegativity difference as a factor for evaluating the thermal stability of Al-rich metallic glasses, Philos. Mag. Lett. 88 (2008) 917–924.

[9] Z.P. Chen, J.E. Gao, Y. Wu, H. Wang, X.J. Liu, Z.P. Lu, Designing novel bulk metallic glass composites with a high aluminum content, Sci. Rep. UK (2013) 3–12.

[10] S.F. Chen, C.Y. Chen, C.H. Lin, Insight on the glass-forming ability of Al–Y–Ni–Ce bulk metallic glass, J. Alloys Compd. 637 (2015) 418–425.

[11] S. Gonzalez, J. Sort, D.V. Louzguine-Luzgin, J.H. Perepezko, M.D. Baro, A. Inoue, Tuning the microstructure and mechanical properties of Al-based amorphous/crystalline composites by addition of Pd, Intermetallics 18 (2010) 2377–2384.

[12] K.G. Prashanth, H. Shakur Shahabi, H. Attar, V.C. Srivastava, N. Ellendt, V. Uhlenwinkel, et al., Production of high strength $Al_{85}Nd_8Ni_5Co_2$ alloy by selective laser melting, Addit. Manuf. 6 (2015) 1–5.

[13] X.P. Li, C.W. Kang, H. Huang, L.C. Zhang, T.B. Sercombe, Selective laser melting of an $Al_{86}Ni_6Y_{4.5}Co_2La_{1.5}$ metallic glass: processing, microstructure evolution and mechanical properties, Mater. Sci. Eng. A 606 (2014) 370–379.

[14] X.P. Li, C.W. Kang, H. Huang, T.B. Sercombe, The role of a low-energy-density re-scan in fabricating crack-free $Al_{85}Ni_5Y_6Co_2Fe_2$ bulk metallic glass composites via selective laser melting, Mater. Des. 63 (2014) 407–411.

[15] N.C. Wu, D. Kan, L. Zuo, J.Q. Wang, Efficient atomic packing-chemistry coupled model and glass formation in ternary Al-based metallic glasses, Intermetallics 39 (2013) 1–4.

[16] N.C. Wu, M. Yan, L. Zuo, J.Q. Wang, Correlation between medium-range order structure and glass-forming ability for Al-based metallic glasses, J. Appl. Phys. 115 (2014) 043523.

[17] K.J. Laws, B. Gun, M. Ferry, Influence of casting parameters on the critical casting size of bulk metallic glass, Metall. Mater. Trans. A 40A (2009) 2377–2387.

[18] J.H. Perepezko, K. Hildal, Analysis of solidification microstructures during wedge-casting, Philos. Mag. 86 (2006) 3681–3701.

[19] Y.J. Kim, R. Busch, W.L. Johnson, A.J. Rulison, W.K. Rhim, Experimental determination of a time-temperature-transformation diagram of the undercooled $Zr_{41.2}Ti_{13.8}CU_{12.5}Ni_{10.0}Be_{22.5}$ alloy using the containerless electrostatic levitation processing technique, Appl. Phys. Lett. 68 (1996) 1057–1059.

[20] P.T. Sarjeant, R. Roy, A new approach to prediction of glass formation, Mater. Res. Bull. 3 (1968) 265.

[21] A. Takeuchi, A. Inoue, Quantitative evaluation of critical cooling rate for metallic glasses, Mater. Sci. Eng. A 304-306 (2001) 446–451.

[22] N. Yodoshi, R. Yamada, A. Kawasaki, A. Makino, Evaluation of critical cooling rate of $Fe_{76}Si_9B_{10}P_5$ metallic glass by containerless solidification process, J. Alloys Compd. 643 (2015) S2–S7.

[23] J.H. Lienhard IV, L. VJH, A Heat Transfer Textbook(Cambridge massachussets) 2006.

[24] X.J. Wang, X.D. Chen, T.D. Xia, W.Y. Yu, X.L. Wang, Influencing factors and estimation of the cooling rate within an amorphous ribbon, Intermetallics 12 (2004) 1233–1237.

[25] S. Guo, Y. Liu, Estimation of critical cooling rates for formation of amorphous alloys from critical sizes, J. Non-Cryst. Solids 358 (2012) 2753–2758.

[26] A. Takeuchi, A. Inoue, Calculations of mixing enthalpy and mismatch entropy for ternary amorphous alloys, Mater. Trans. JIM 41 (2000) 1372–1378.

[27] H.J. Fecht, Thermodynamic properties of amorphous solids—glass formation and glass transition, Mater. Trans. 36 (1995) 777–793.

[28] A.F. Ilkhchy, N. Varahraam, P. Davami, Evaluation of pressure effect on heat transfer coefficient at the metal-mold interface for casting of A_{356} Al alloy, Iran. J. Mater. Sci. Eng. 9 (2012) 11–20.

[29] M. Trovant, S.A. Argyropoulos, The implementation of a mathematical model to characterize mold metal interface effects in metal casting, Can. Metall. Q. 37 (1998) 185–196.

[30] J. Schroers, W.L. Johnson, R. Busch, Crystallization kinetics of the bulk-glass-forming $Pd_{43}Ni_{10}Cu_{27}P_{20}$ melt, Appl. Phys. Lett. 77 (2000) 1158–1160.

[31] J. Schroers, Processing of bulk metallic glass, Adv. Mater. 22 (2010) 1566–1597.

[32] L.C.R. Aliaga, G.P. Danez, C.S. Kiminami, C. Bolfarini, W.J. Botta, Topological instability and glass forming ability of Al–Ni–Sm alloys, J. Alloys Compd. 509 (2011) S141-S4.

[33] F.Q. Guo, S.J. Poon, G.J. Shiflet, Investigation of glass formability in Al-based multinary alloys, Scr. Mater. 43 (2000) 1089–1095.

[34] B.J. Yang, J.H. Yao, Y.S. Chao, J.Q. Wang, E. Ma, Developing aluminum-based bulk metallic glasses, Philos. Mag. 90 (2010) 3215–3231.

[35] Z. Zhang, W. Zhou, X.Z. Xiong, L.T. Kong, J.F. Li, Glass forming ability and primary crystallization behavior of Al–Ni–Ce alloys, Intermetallics 24 (2012) 1–6.

[36] P. Dong, J. Zhang, W.L. Hou, X.C. Chang, J.Q. Wang, Investigation of glass formability in Al–Co–Y ternary system, J. Mater. Sci. Technol. 24 (2008) 161–164.

[37] W.S. Sanders, J.S. Warner, D.B. Miracle, Stability of Al-rich glasses in the Al–La–Ni system, Intermetallics 14 (2006) 348–351.

[38] Y. He, G.M. Dougherty, G.J. Shiflet, S.J. Poon, Unique metallic glass formability and ultra-high tensile strength in Al–Ni–Fe–Gd alloys, Acta Metall. Mater. 41 (1993) 337–343.

[39] R. Busch, J. Schroers, W. Wang, Thermodynamics and kinetics of bulk metallic glass, MRS Bull. 32 (2007) 620–623.

[40] H.W. Yang, P. Dong, J.Q. Wang, Y. Li, Glass formability and structural stability of Al-based alloy systems, Mater. Sci. Eng. A 449-451 (2007) 273–276.